Korean J. Chem. Eng., 38(8), 1617-1630 (2021)
DOI: 10.1007/s11814-021-0819-z

pISSN: 0256-1115
eISSN: 1975-7220

Techno-economic feasibility evaluation of a standalone solar-powered alkaline water electrolyzer considering the influence of battery energy storage system: A Korean case study

Haider Niaz, Mohammad MansourLakouraj, and Jay Liu†

Department of Chemical Engineering, Pukyong National University, Busan 48513, Korea
(*Received 23 January 2021 • Revised 20 April 2021 • Accepted 23 April 2021*)

Abstract−Hydrogen use is dominated by industry, with most hydrogen demand mitigated using fossil fuels; therefore, there is an eminent potential for the reduction of emissions by replacing fossil-derived hydrogen with a renewable hydrogen source. Although the emission reduction by using renewable energy presents a promising potential, its fluctuating nature is still a challenge to be addressed. In this study, considering a battery energy storage system (BESS), a dynamic operation-based techno-economic evaluation of a standalone solar photovoltaic (PV)-powered alkaline water electrolyzer (AWE) was conducted using actual solar data. Different process configurations were designed and simulated to quantify the available potential of a standalone solar-powered hydrogen production system in Korea. Furthermore, economic evaluation metrics, such as levelized cost of hydrogen (LCOH) and Monte Carlo simulation, were used to assess the potential of different configurations under variable market prices and future technology costs to estimate the future potential. The results showed that Case 1 (standalone solar-powered AWE without BESS) offers the lowest LCOH (9.55 $/kg) but with daytime operation only. Meanwhile, Case 4 (standalone solar-powered AWE with BESS) reported the second-lowest LCOH (11.67 $/kg) compared with the other cases. The results also suggested that systems with BESS can increase operational reliability by minimizing operational fluctuations and maximizing operational hours but with a slightly higher LCOH. The conducted sensitivity analysis showed that the technology cost (solar PV, AWE, and BESS) has the highest impact on LCOH, which is promising, in light of the decreasing trend in the future costs of such technologies.

Keywords: Alkaline Water Electrolyzer, Solar Power, Battery Energy Storage System, Techno-economic Analysis, Levelized Cost Of Hydrogen

INTRODUCTION

The increasing global CO_2 emissions and current climate challenges urge a significant transition to increase the usage of renewable energy sources [1,2]. Especially, countries whose primary energy supply mainly depends on fossil fuels, such as the Republic of Korea, face serious challenges in regard to reducing greenhouse gas emissions (GHG) under the Paris agreement [3]. While the implementation of renewable energies is expanding in the Republic of Korea, further expansion requires storage and power conversion technologies to compensate for the intermittent nature of renewable energy [4-6]. Battery energy storage systems (BESS) can be considered as short-term storage systems, but they do not form a viable alternative to long-term storage systems owing to their high capital costs. However, BESS can assist in the operation of power systems with the integration of renewables. In addition, they can minimize the instability induced by the fluctuating nature of renewable energy and provide an alternate means of energy storage.

Hydrogen has the potential to decarbonize energy-intensive industries. However, its decarbonization impact depends on the hydrogen production method. Currently, the available hydrogen production options can be divided into three categories: gray (fossil fuel-based), blue (fossil fuel-based with carbon capture), and green hydrogen (renewable based) [7-10]. Among them, the green hydrogen produced via renewable-energy-powered electrolysis is expected to rapidly grow in the coming years. The recent development in electrolysis technology offers high production capacity and the ability to operate at low loads. Moreover, hydrogen production via the integration of renewable energy with the commercially available alkaline water electrolyzer (AWE) technology can be a promising alternative for large-scale energy storage, possibly avoiding the installation of huge BESS, eventually saving more costs [11]. However, combining BESS and highly intermittent energy sources, such as solar photovoltaic (PV) cells and wind turbines, with electrolyzers to produce hydrogen gas might offer great operational reliability but with additional cost [12,13].

The commercial-scale implementation of renewable hydrogen has to be economically viable as compared with other conventional hydrogen production means, such as steam methane reforming [14]. Considering renewable electricity as a primary raw material, the generation cost of renewable electricity significantly impacts the levelized cost of hydrogen (LCOH) ($/kg) and greatly depends on the renewable energy source. With advancements in solar technology, the cost of solar generated electricity sharply declined (77%)

†To whom correspondence should be addressed.
E-mail: jayliu@pknu.ac.kr

from the original cost in 2010 over 2010-2019 and became cheaper than wind-generated electricity [15]. In this regard, along with an operational strategy that leads to fluctuation reduction, improved flexibility, and LCOH minimization ($/kg), the combination of solar photovoltaic (PV) powered AWE with BESS can be a reliable hydrogen production system. However, there are no long-term supporting studies for such operation concepts.

Techno-economic assessment studies are rather generalized based on the average yearly, monthly, or weekly solar data without considering the technical limitations of electrolyzers in dynamic operation in detail. In Germany, Ulleberg presented a dynamic PV-hydrogen model with a battery and grid support; however, an economic evaluation was not provided [16] and the author did not account for excess power generation. Gallardo et al. presented a techno-economic analysis of solar hydrogen production by electrolysis [17]. They used an average seasonal profile for solar power generation to evaluate LCOH and quoted a price as low as 2.20 $/kg with a power purchase agreement (PPA) [17]. Despite the agreement policy, the provided low hydrogen costs are too optimistic in light of the current technology costs. Gutierrez-Martin et al. presented an off-grid hydrogen production system and compared the options with and without BESS at different locations, where the power constraints of the off-grid locations were avoided and average monthly days of the solar radiation data were used [18]. Several further studies [11,19-23] investigated the production of hydrogen via renewable energy systems and assessed cost of hydrogen production at various scales. Countries with higher solar power generating potential tend to report lower LCOH. In this regard, Grimm et al. reported an LCOH of 6.22 $/kg using PV and a proton exchange membrane (PEM) electrolyzer based on the climate of the Netherlands [24]. Martin et al. reported an LCOH of 6.42 and 6.68 $/kg for with and without BESS via AWE and PV [18]. However, LCOH based on 100% renewable-energy-powered systems for the Korean case scenario is still scarce. Other studies reported LCOH based on grids with electricity-powered electrolyzers [25,26]. Recent studies on hydrogen systems have reported the LCOH for different electrolysis technologies with and without grid support, and with and without BESS. More information regarding this can be found in Table 1. The reported LCOH values had a wide variation. New results have indicated that seasonal variations and geography affect the overall performance of these plants [27]. Higher costs have been reported for countries with fewer sunshine hours than those with more sunshine hours. However, these studies failed to consider replacement costs or greater time resolution and analyzed average values or short periods instead. Therefore, the reported values may appear good on paper but they do not reflect any realistic estimate associated with such processes.

Overall, there is a lack of detailed techno-economic assessments based on the dynamic operation of 100% renewable and standalone AWEs that are coupled with BESS and are based on actual one-year solar data that incorporate the effects of seasonal and daily fluctuations. To the best of authors' knowledge, no study has yet reported any dynamic operation-based techno-economic evaluations of green hydrogen production via standalone solar-powered AWE with and without BESS for the Korean case scenario. Therefore, in this study, a techno-economic analysis based on the dynamic operation of a solar-powered AWE with and without BESS was modeled using actual weather data from the system advisor model (SAM) for the whole year of 2018 with one-hour time interval [28]. The model presents an operational strategy that considers the operational capacity of both AWE and BESS and minimizes the operational fluctuations and frequent startups and shutdowns due to fluctuating PV energy. In addition, the model provides insight into a precise energy and mass balance model for the operation of water electrolysis, BESS's state of charge (SOC), and hydrogen storage when subjected to renewable energy for one year. Most importantly, the model uses actual weather data of the Republic of Korea to assess the solar AWE-based hydrogen production potential as supporting material for future investors and policymakers. To better understand the economic potential of solar-powered AWE and BESS, design cases were developed for an AWE powered by a solar power plant with and without BESS. Sensitivity analysis and Monte Carlo simulation were performed to assess the future investment risk to cover the expected market fluctuation and estimate the expected LCOH range. Thus, a comprehensive techno-economic-based dynamic operation of a standalone solar-powered AWE was presented with a focus on the economic and technical aspects of green hydrogen production.

Table 1. Recent literature on LCOH for AWE and PEM with/without grid support and with/without BESS

Sr. No	Electrolyzer	BESS	Grid	LCOH ($/kg)	Country	Average sunshine hours	Reference
1	AWE, PEM	-	-	7.21, 9.19	Korea	5.66 h	[46]
2	AWE	-	Yes	4.96-5.78	USA	8.14 h	[47]
3	AWE	-	-	7.14	UK	4.5 h	[48]
	AWE	-	Yes	8.09	UK		
4	PEM	-	-	11	Australia	8 h	[48]
5	PEM	-	-	5.8	Morocco	11 h	
6	AWE	-	-	6.72	Italy	6.46 h	[18]
	AWE	Yes		8.12			
7	PEM	No	-	18.67	Australia	8 h	[49]
	PEM	Yes	-	28.43			
	PEM	No	-	9.14			
	PEM	Yes	-	11.31			

MODEL DESCRIPTION

Applying electric current to water causes it to dissociate into hydrogen and oxygen in the presence of a suitable electrolyte. The water splitting can be represented as follows:

$$H_2O_{(l)} + \text{electrical energy} \rightarrow H_{2(g)} + 0.5 \times O_{2(g)} \quad (1)$$

For the reaction (Eq. (1)) to occur, a minimum amount of reversible electrical voltage is required, which can be calculated from the Gibbs energy formula for water splitting [16]. The anodic and cathodic reactions taking place are explained as follows:

$$\text{Anode: } 2OH^-_{(aq)} \rightarrow 0.5 \times O_2(g) + H_2O_{(l)} + 2e^- \quad (2)$$

$$\text{Cathode: } 2H_2O_{(l)} + 2e^- \rightarrow H_{2(g)} + 2OH^-_{(aq)} \quad (3)$$

The chemical Eqs. (2)-(3) require a specific voltage to dissociate water into hydrogen and oxygen. On applying this voltage across the ends of the positive and negative electrodes, the minimum voltage results in hydrogen production. The minimum electric voltage (reversible voltage (V_{rev})) can be determined using the Gibbs Eq. (4), where ΔG=Gibbs energy, z=number of electrons, and F=Faraday's constant [16].

$$\Delta G = z \times F \times V_{rev} \quad (4)$$

$$V_{rev} = \frac{\Delta G}{z \times F} \quad (5)$$

$$V_{rev} = \left(237.2 \frac{kJ}{Kmol}\right) / \left(2 \times 96{,}485 \frac{C}{mol}\right) = 1.229V \quad (6)$$

In electrolysis, the operating cell voltage is the total of the reversible voltage, activation voltage (V_{act}), and ohmic overvoltage (V_{ohm}) of the electrolyte. To generate hydrogen from electric power, both the ohmic loss and overvoltage increase with the increase in current density and raise the cell voltage value. This equation can be represented as follows:

$$V_{cell} = V_{rev} + V_{act} + V_{ohm}. \quad (7)$$

The relations in Eq. (7) can be expressed as follows:

$$V_{act} = s \times \log(I \times ((t_1 + (t_2/T) + (t_3/T^2))/A) + 1), \quad (8)$$

$$V_{ohm} = ((r_1 + r_2 \times T)/A) \times I. \quad (9)$$

Using these correlations, Eq. (7) can be rewritten as Eq. (10) to consider the ohmic resistance and overpotential, as suggested by Ulleberg [16].

$$V_{cell} = V_{rev} + s \times \log((I \times ((t_1 + (t_2/T) + (t_3/T^2))/A)) + 1) + ((r_1 + r_2 T)/A) \times I \quad (10)$$

Here, s is the coefficient for the overvoltage on electrodes (V), t, t_1, t_2, t_3 are the coefficients for the overvoltage on the electrodes (A^{-1} m^2), T is the temperature (°C), A is the area of the electrode (m^2), I is the current (A), and r_1, r_2 are the parameters related to the ohmic resistance of the electrolyte (Ωm^2). Based on Faraday's law of electrolysis, the amount of hydrogen produced is proportional to the amount of electron transfer. The Faraday efficiency can be defined as the ratio between the actual and calculated amounts of hydrogen:

$$\eta_F = ((I/A)^2/(f_1 + (I/A)^2)) \times f_2. \quad (11)$$

where η_F is the Faraday efficiency of the electrolyzer and f_1, f_2 are parameters related to the Faraday efficiency of the electrolyzer (mA^2 cm^{-4}). The hydrogen production rate (Nm^3/h) in an electrolyzer with a series of cells can be calculated using the following equation:

$$H_2^{GEN} = \eta_F \times ((n_c \times I)/(z \times F)) \quad (12)$$

n_c is the number of cells in series per stack, z is the number of electrons per reaction, and F is the Faraday constant (96,485 $Cmol^{-1}$). The formulation in Eq. (12) can be converted into Eq. (12a) [29, 30]. Cells constituting the stack are identical. Thus, a stack with n_c cells can be modeled as an equivalent to a single cell that has the same dynamics as the whole stack. Therefore, n_c can be neglected. Additionally, because P=V×I, substituting I=P/V into Eq. (12) we get,

$$H_2^{GEN} = \eta_F \times ((P)/(V \times z \times F)) \quad (12a)$$

(V×z×F) is equal to ΔH (LHV) of hydrogen [16], so substituting this into Eq. (12a) we get,

$$H_2^{GEN} = \eta_F \times (P/LHV) \quad (12b)$$

Because the overall electrolyzer efficiency depends both on the Faraday efficiency and overpotential (i.e., difference between the theoretical and actual voltages), we can replace η_F with η_{Ele}. Thus, Eq. (12b) can be rewritten as

$$H_2^{GEN} = \frac{\eta_{Ele} \times P}{LHV} \quad (12c)$$

where η_{Ele} is the electrolyzer efficiency, P is the power to the electrolyzer, and LHV is the lower heating value of hydrogen. The production rate for the oxygen and water consumption can be calculated using stoichiometry as shown below:

$$H_2O^{cons} = H_2^{GEN} = 0.5 \times O_2^{GEN} \quad (13)$$

H_2O^{cons}, H_2^{GEN}, O_2^{GEN} are the water consumed, hydrogen generated, and oxygen generated, respectively. The volumetric hydrogen flow rate (Q) in Eq. (12) can be converted to the unit of kg/h as follows:

$$Q = ((H_2^{GEN} \times 3{,}600 \times 0.022414)/(11.1)).$$

The term (3,600×0.022414)/(11.1) converts the volumetric flow rate into a mass flow rate.

1. Dynamic Modeling

1-1. Solar PV for Hydrogen Production

The solar irradiation data of Incheon Korea was obtained from SAM [28] and used to generate the current, voltage, and power profiles of a 6.5-MW PV system. The solar power production model by SAM takes the following assumptions:

(a) The solar PV modules are operated in a shadow-free environment.

(b) The solar panels considered in this analysis were designated as SunPower SPR-X21-350-BLK-E-AC, and their technical details are shown in Table 2 [28].

(c) The PV system is standalone with no connection to the grid.

(d) The solar PV modules only supply electricity to the electro-

Table 2. Electrical data measured at standard test conditions (STC)

Category	Unit	1,000 W/m^2
Nominal power	W	350.103
Rated voltage	V	57.3
Rated current	A	6.11
Open circuit voltage	V	68.2
Short circuit current	A	6.5
Number of solar cells		96

lyzer plant. The additional electrical requirements for the office and control systems were not considered in this analysis.

The technical details of the weather data, solar module, inverter, and system design for the solar panel can be seen in Table S1 (supplementary data). The solar irradiation data for one year with one-hour time interval, as shown in Fig. S1 (supplementary data), was used to generate power from a 6.5-MW solar plant. In 2018, from April to August, the hot months, the peak solar irradiation ranged from ~610 to ~700 W/m^2, whereas the cold months from October to January had the lowest irradiation in comparison with the hot months. However, February, September, and March had irradiation range between the hot and cold months.

1-2. Alkaline Water Electrolyzer

The general equations representing the phenomena taking place at the anode and cathode can be written as follows, as shown in Eq. (14) and (15) and Eq. (16) and (17), respectively:

$$\frac{dH_2O}{dt} = H_2O^{IN} - H_2O^{OUT} + H_2O^{GEN}, \quad (14)$$

$$\frac{dO_2}{dt} = O_2^{IN} - O_2^{OUT} + O_2^{GEN}, \quad (15)$$

where H_2O^{IN}, H_2O^{OUT}, O_2^{IN}, O_2^{OUT} are the anode inlet and outlet mass flow rates of water and oxygen, respectively, and H_2O^{GEN}, O_2^{GEN} are the mass flow rates of the water and oxygen generated at the anode, respectively.

$$\frac{dH_2O}{dt} = H_2O^{IN} - H_2O^{OUT} + H_2O^{CONS}, \quad (16)$$

$$\frac{dH_2}{dt} = H_2^{IN} - H_2^{OUT} + H_2^{GEN}, \quad (17)$$

where H_2O^{IN}, H_2O^{OUT}, H_2^{IN}, H_2^{OUT} are the anode inlet and outlet mass flow rates of water and hydrogen, respectively, and H_2O^{CONS}, H_2^{GEN} are the mass flow rates of the water consumed at the cathode and the hydrogen generated at the cathode, respectively.

H_2^{GEN} can be expressed as follows:

$$H_2^{GEN}(t) = \frac{\eta_{Ele} \times P(t)}{LHV}. \quad (18)$$

1-3. Hydrogen Tank

The stored hydrogen (H_2^{STO}) amount can be represented by Eq. (19) given as follows:

$$H_2^{STO}(t) = \int_0^t H_2^{GEN}(t')dt'. \quad (19)$$

1-4. Battery Energy Storage System

A battery energy storage system must supply and store power during night and day, respectively. The BESS is charged via solar power during the day when ample sunlight is available. Later, in the absence of sunlight, BESS takes over and supplies constant power to the electrolyzer. The battery's SOC defines the available energy in the battery. To preserve the battery life and protect BESS, operational constraints were applied to the model, as shown in Eq. (20)-(23).

$$P_C(t) \times P_D(t) = 0 \quad (20)$$

$$P_{C_{MIN}} \le P_C(t) \le P_{C_{MAX}} \quad (21)$$

$$P_{D_{MIN}} \le P_D(t) \le P_{D_{MAX}} \quad (22)$$

$$SOC_{MIN} \le SOC(t) \le SOC_{MAX} \quad (23)$$

P_C is the charging power of BESS, and $P_{C_{MIN}}$ (0 kW) and $P_{C_{MAX}}$ (1,000 kW) are the minimum and maximum charging power of BESS, respectively. P_D is the power discharged from BESS, $P_{D_{MIN}}$ is the minimum discharge power from BESS, and $P_{D_{MAX}}$ is the maximum discharge power from BESS. To avoid any identity conflicts, a new variable cn was used. The value of cn was fixed at any given time and was chosen as a varying value for the different cases discussed in this study. It may have a different value chosen between $P_{D_{MIN}}$ (0 kW) and $P_{D_{MAX}}$ (1,000 kW). SOC is the SOC of BESS, and SOC_{MIN}, SOC_{MAX} represent the minimum and maximum SOC levels, respectively. In this study, SOC_{MIN}, SOC_{MAX} were 30% and 100% of the BESS rated capacity, respectively. SOC(t) could be represented at any given time, as shown in Eq. (24).

$$SOC(t) = SOC(t - \Delta t) + ((\eta^+ \times P_C(t)) - (\eta^- \times P_D(t)))\Delta t, \quad (24)$$

where η^+, η^- are the charging and discharging efficiency, and the initial value of SOC was 100% of the BESS rated capacity. The charging and discharging efficiency were considered (5% loss).

2. Dynamic Operation Strategy

The data used to model the electrolyzer is shown in Table S2 (supplementary data). The values of the parameters used in this model were from literature [16,31]. The gPROMS platform was used to model the dynamic equations for the AWE. The simulation was run for four different conditions: solar AWE without BESS (Case 1), solar AWE and BESS with a dynamic operation strategy and a fixed discharge power from BESS (Case 2), solar AWE with BESS with an operational strategy and variable discharged power from BESS (Case 3), and solar AWE with BESS and maximum discharge power from BESS (Case 4). A simple block diagram can be seen in Fig. 1, where (a) represents Case 1, and (b) represents Cases 2-4. Case 1 includes a solar system with AWE and a hydrogen storage option, whereas Cases 2-4 consist of a solar system, AWE, a BESS, and a hydrogen storage unit. For ease of understanding, Cases 3 and 4 are similar to Case 2, and the only difference between Cases 2, 3, and 4 is the discharged power from BESS.

Battery energy storage system is an alternate energy provider that stores energy during renewable energy availability and then discharges it when there is no or less renewable energy availability. Furthermore, it helps in minimizing the fluctuations imposed by renewable energy sources. Although BESS can help reduce solar

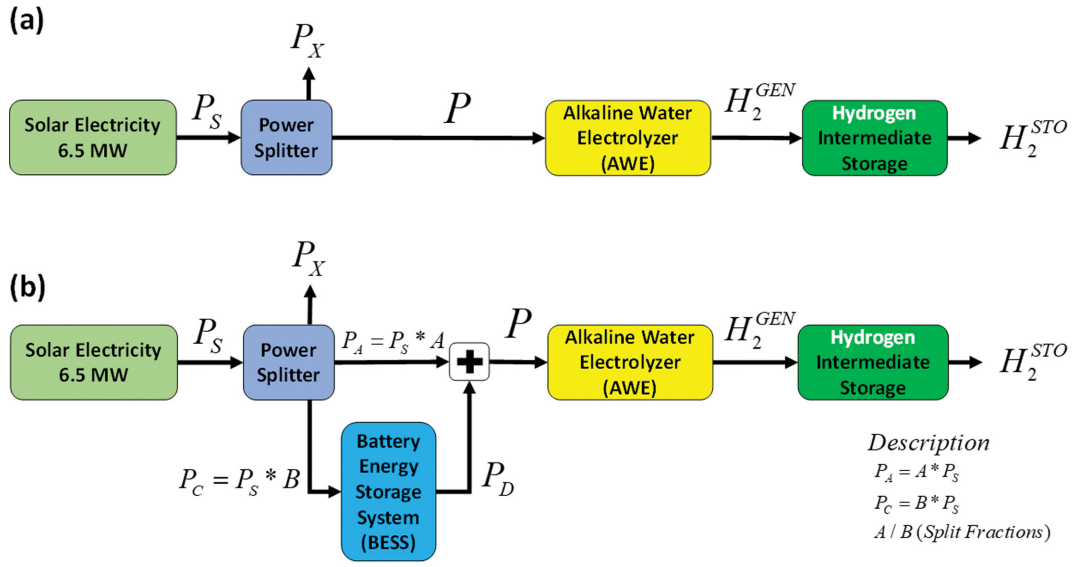

Fig. 1. Block diagram of alkaline water electrolyzers (AWEs) (a) without (Case 1) and (b) with (Case 2) a battery energy storage system (BESS).

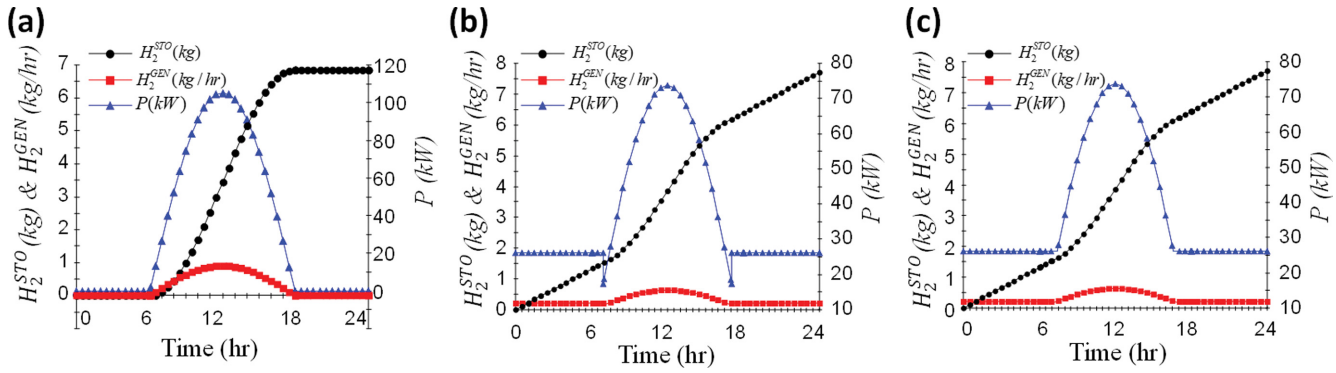

Fig. 2. Operation of (a) Case 1 and (b) Case 2 without the proposed operational strategy and (c) Case 2 with the proposed operational strategy.

power input fluctuations by providing support and supplying power to AWEs during daytime, a problem still exists in controlling the amount of the charged and discharged power from BESS. Furthermore, the shift from BESS power to solar generated power at the start of daytime creates disturbances, which should be minimized and controlled for the smooth transition from BESS power to solar power and vice versa. Without any proper operation strategy, disturbances may take place, thus hindering the utilization of BESS and resulting in its overcharging and discharging, eventually reducing its lifetime.

In Case 1, as shown in Fig. 1(a), solar power (P_S) is fed to AWE, which takes the required power (P) for its operation, and the supplementary power is assumed to be sold to the neighboring industries. Whereas for Case 2, the solar power (P_S) generated from the solar plant is split into two fractions: (A) and (B), as shown in Fig. 1(b). These fractions are set at different ratios. In this model, (A) is 0.7, and (B) is 0.3, where their sum is always equal to 1.0. P_S is split into two power streams: P_A=P_S×A and P_C=P_S×B, respectively. P_A is the power going to AWE, P_C is the power going to BESS to charge the batteries, P_D is the power discharged from the BESS and P_X is the supplement power, which is assumed to be sold to neighboring industries when neither AWE nor BESS needs any more power (i.e., operating at maximum load and BESS is fully charged). The total power fed to AWE is equal to P, i.e., P=P_A+P_D.

To understand the operational difference between Case 1 and Case 2, simple graphs are demonstrated in Fig. 2(a) and (b), respectively, at standard solar irradiation, 1,000 W/m^2. A typical day was assumed with 12 h of daylight from 06:00 to 18:00. Fig. 2(a) illustrates the operation of Case 1. The power to AWE (P) (blue line) is zero from 00:00 to 06:00. Then, it increases toward the peak from 06:00 to 12:00, and from 12:00 to 18:00, it gradually falls to zero; from 18:00 to 24:00, it remains zero (i.e., no power to produce hydrogen) evidently due to the absence of solar energy. Therefore, AWE is operational only during daytime, which is why the hydrogen production rate H_2^{GEN} (kg/hr) (red line) is zero from 00:00 to 06:00 and from 18:00 to 24:00. Similarly, the total hydrogen production (H_2^{STO} (kg)) (black line) is zero from 00:00 to 06:00, but it then increases from 06:00 to 18:00. Afterward, it becomes zero again, as shown by the stagnant line.

However, in Case 2, it can be seen from Fig. 2(b) that during the entire operation course, AWE is operational for 24 h. This is because BESS provides power to AWE during the night: 00:00 to 06:00 and

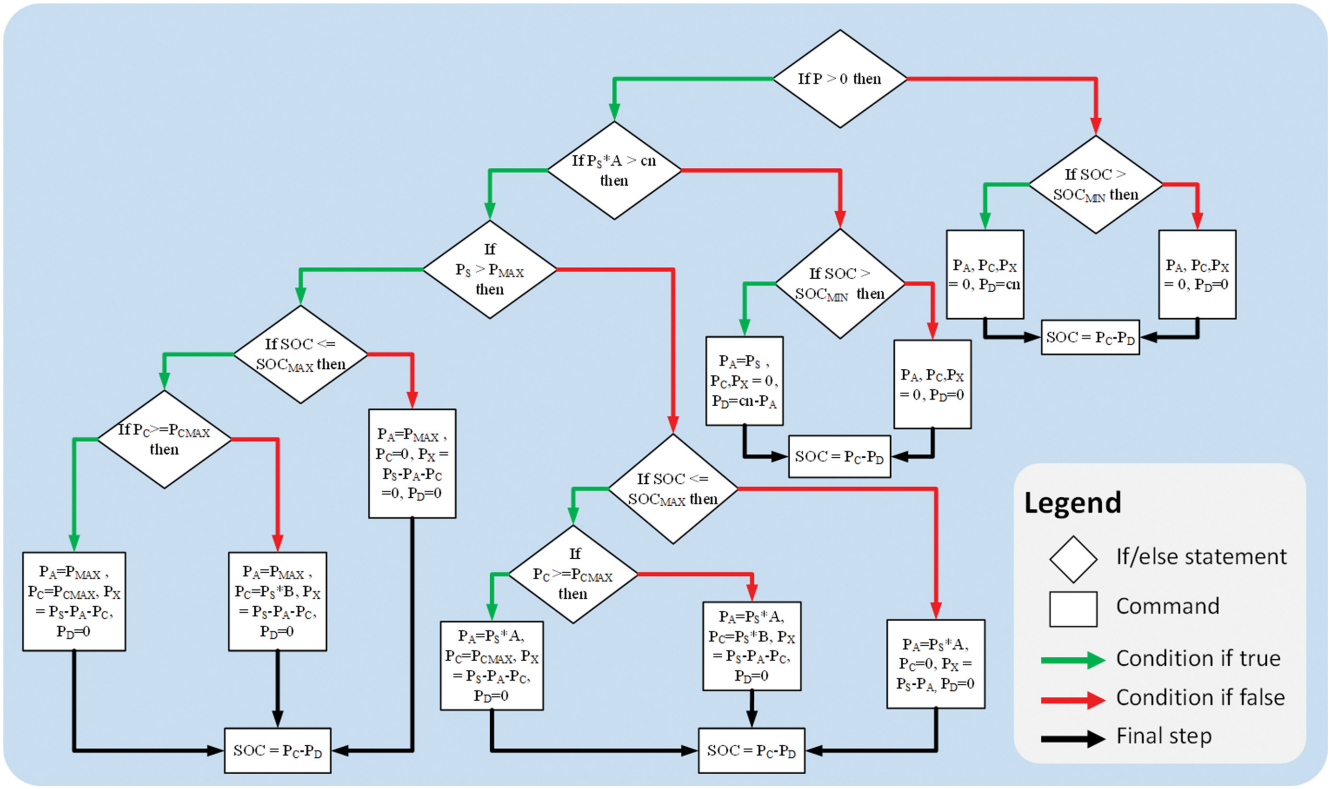

Fig. 3. Flowchart of the dynamic operational strategy for Cases 2-4.

18:00 to 24:00. Nevertheless, it can be observed that there are downward spikes in the power (P) at dawn and dusk in Fig. 2(b), which are the operational disturbances when shifting from BESS to solar power and vice versa. The reason behind these spikes is that AWE starts taking power from the solar power directly once the day begins, and the discharge power (P_D) from BESS is higher than the solar power (P_S). Due to the higher power value (P_D) of BESS, the shift to solar power creates an operation spike, thus creating an operational disturbance.

To overcome these disturbances, an operational strategy that ensures smooth shifts from BESS to direct solar power and vice versa and that guarantees the safe operation of BESS was proposed. A simple flowchart that supports smooth operation and explains the operational strategies of Cases 2-4 can be seen in Fig. 3. The solar power (P_S) value decides the switching between day and night, followed by controls, which choose whether power should be split into P_A, P_C, or P_X. In addition, they can also determine if all P_S needs to go directly to AWE. The operation strategy works in the following pattern.

1- If P_S is equal to zero, shift to night. P_A, P_C, P_X=0. Check if SOC<SOC_{MIN} (30% of the total SOC capacity). If yes, set P_D=0, otherwise, P_D=<*value of current during night* (*cn*)>

2- If P_S is greater than zero and P_A is less than cn, all the power directly goes to AWE. BESS provides the remaining power to support the AWE operation until P_S is greater than P_{MIN} (10% of the rated AWE capacity). Check if *SOC is greater than* SOC_{MIN}. If yes, set $P_D=c_n-P_A$, otherwise, P_D=0.

3- If P_S is greater than zero, P_A is greater than cn, and P_S is less than the maximum AWE power capacity (P_{MAX}) (100% of the total AWE capacity). Check if SOC≤SOC_{MAX} (100% of the total BESS capacity). If yes, check if $P_C \geq P_{C_{MAX}}$. If yes, set $P_A=P_S \times A$, $P_C=P_{C_{MAX}}$, P_D=0, $P_X=P_S-P_A-P_C$, otherwise, set the values as $P_A=P_S \times A$, $P_C=P_S \times B$, P_D=0, and $P_X=P_S-P_A-P_C$. Now, if SOC≥SOC_{MAX}, set $P_A=P_S \times A$, P_C, P_D=0, $P_X=P_S-P_A-P_C$. In all cases, P_X is only applicable when the power exceeds the upper limit of AWE, BESS, or both (i.e., P_{MAX} and SOC_{MAX}) to ensure the maximum utilization of the available solar power. P_X has a lower limit of zero and an upper limit of P_S (i.e., $0 \leq P_X \leq P_S$).

4- If P_S is greater than zero, P_A is greater than cn, and P_S is greater than the maximum AWE power capacity (P_{MAX}). Check if SOC≤ SOC_{MAX} (100% of the total BESS capacity). If yes, check if $P_C \geq P_{C\_MAX}$. If yes, set $P_A=P_{MAX}$, $P_C=P_{C_{MAX}}$, P_D=0 and $P_X=P_S-P_A-P_C$, otherwise, set the values as $P_A=P_{MAX}$, $P_C=P_S \times B$, P_D=0, and $P_X=P_S-P_A-P_C$. Now, if SOC≥SOC_{MAX}, set $P_A=P_{MAX}$, P_C, P_D=0 and $P_X=P_S-P_A-P_C$.

5- All the above mentioned conditions are followed by a common step, i.e., $P=P_A+P_D$, and by Eq. (18) and (19).

Fig. 2(c) illustrates the operation for Case 2. The spikes seen in Fig. 2(b) at 06:00 and 18:00 were addressed and a smooth shift from BESS to solar power was achieved. The proposed operational strategy ensured that solar power only takes over if the solar generated power is greater than the one supplied by BESS. Furthermore, when there is less solar power generation, BESS provides supplement power in addition to solar generated power to ensure minimum load operation. In addition, during the times when there was excess power remaining, the power was considered as power

to be sold, thus maximizing the utilization of the available energy and resources.

3. Techno-economic Analyses

The year 2020 was taken as a basis for the analyses. The techno-economic model was similar to the one used by Turton et al. [32]. The raw materials (deionized water, nitrogen, steam, and KOH) consumption per kg of produced hydrogen were estimated using the ones quoted in National Renewable Energy Laboratory (NREL) report [33]. The AWE cost was taken from the report by Bertuccioli et al. [34], and the cost for the stack replacement was also considered. The cost of the storage and compression equipment was taken from NREL [35]. The total capital investments were calculated according to the report by Turton et al. [36]. The latest costs for the available solar and BESS technology were taken from "Annual Technology Baseline: Electricity" for the year 2020 [37]. The report covers the current and future projected costs for the solar and BESS technology. The selling price for excess power was taken as 0.098 $/kWh based on the Korean market price [38], and the oxygen selling price was taken as 0.18 $/kg. The total installation costs included the building, additional piping, and site development costs, and the percentages of these factors were taken from Turton et al.'s study [39]. All the equipment and raw material costs were adjusted based on the chemical engineering plant cost index (CEPCI) owing to the difference in the quoted price year. The CEPCI for 2020 was taken as 599.5 [40], and the current-year costs (X) were calculated as shown in Eq. (25).

$$\text{Cost in Current Year (X)} = \text{Cost in Quoted Year (Y)} \times \frac{\text{Current year cost index (2020)}}{\text{Quote year cost index (CI)}} \quad (25)$$

The plant life was assumed to be 30 years with an IRR of 4.5%. Our study's startup time was taken as 0.5 year with a working capital equivalent to 5% of the fixed capital investment (FCI). The construction period for our case is one year. The base parameters used in the techno-economic model are shown in Table 3. The exact proportion of the allotted percentages for the previously mentioned indirect cost contributors is specified in Table S2 (supplementary data).

Other parameters for calculating FCI are given in Table S3 (supplementary data). The FCI assumptions included direct and indirect costs. The direct costs covered the building (1% of TIC), site development (9% of TIC), and additional piping (4.5% of the TIC) costs for the system. The indirect costs included those of the prorated expenses, office construction, field expenses, project contingency, startups, and permits. The total installed cost was the starting point for calculating the FCI and other operating expenses. All the estimated costs were then used to generate a discounted cash flow analysis to calculate LCOH. Assumptions for the operating costs are discussed in Table S2 (supplementary data) and they include the basic operating costs of the plant. The fixed operating costs include the management and working staff salaries at the plant site, and the variable operating costs include the maintenance, insurance, and tax costs.

Table 3. Parameters of the techno-economic model

Variable	Value
Cost year of analysis	2020
Internal rate of return	10%
Plant financing/debt equity	1
Plant life	30 years
Income tax rate	21%
Startup time	0.5 year
Working capital	5% of fixed capital investment
Construction period	1 year
Plant salvage value	No value
Costs during startup	Variable costs=75% Fixed costs=100%
Indirect capital cost	55% of the TIC

3-1. Levelized Cost of Hydrogen

Levelized cost of hydrogen was calculated using NREL's correlation, as shown in Eq. (26) [41]. The formulation consists of a summation of three terms (capacity cost, operating cost, and maintenance cost) divided by the annual hydrogen production.

$$\text{LCOH} = \left((\text{TLCC} - \text{NPV}_{OP}) / \left(\sum_{0}^{L} \frac{\text{H}_2^{GEN}}{(1+\text{D})^n} \right) \right), \quad (26)$$

where TLCC is the total life cycle cost of the plant, NPV_{OP} is the net present value of the sales revenues of other products (P_X and oxygen), D is the discount rate, n is the analysis year, and L is the analysis period in years (30).

3-2. Sensitivity and Uncertainty Analyses

Levelized cost of hydrogen was subjected to sensitivity analyses using predetermined factors and variation ranges to assess the impact of the parameter fluctuation on the LCOH. The factors included solar CAPEX, AWE CAPEX, discount rate, income tax, deionized water price, storage and compression costs, battery capacity cost, and battery power cost. The ranges for the solar CAPEX, AWE CAPEX, battery capacity cost, and battery power cost were taken from the "Annual Technology Baseline: Electricity" report. The ranges were selected based on the projected future and previous year costs (2017 and 2030) [42]. The ranges for the other parameters, such as the deionized water purchase price (−20% to 10%), discount rate (−10% to 20%), and income tax rate (−20% to 10%) were taken from the study of Dickson et al. [39]. As these parameters vary through their life span, so does LCOH. To assess the uncertainty in the results of the techno-economic analyses, Monte Carlo analysis was performed to determine the most probable LCOH price range by generating a thousand different scenarios of random values of sensitivity parameters. Each scenario generated a different LCOH value. The uncertainty analysis via the Monte Carlo method showed a significant change in LCOH and provided useful insight into the plant economics that must be considered.

RESULTS AND DISCUSSION

1. Model Validation

The AWE model used in this study was validated with the amount of hydrogen produced (kg/h) from the input power (kW) to the electrolyzer, as reported in the study of Kojima et al. [43]. Each cell had an electrode area of 0.25 m^2 and there were 41 cells connected in series. The results were compared with the experimentally re-

Table 4. Validation of the model with the previous study

Power	Literature	Model in this study	Difference
(kW)	(kg/hr)		(%)
15	0.303	0.306	0.96
45	0.902	0.919	1.88
75	1.476	1.532	3.76
105	2.050	2.144	4.59
135	2.624	2.757	5.06

ported values in the literature for the amount of hydrogen produced (kg/hr) at a given power (kW) value. As summarized in Table 4, the difference between the amount of produced hydrogen of the experimental study [43] and that of the current model was very small over the entire input power range, which reflects the model's accuracy and the reliability of this study.

2. Simulation Results

A solar-powered AWE model with a dynamic operational strategy was run for the solar profile data of 2018 of Incheon, Korea. A 4.5-MW AWE (9 sets of 500 kW) and BESS with a power of 1 MW and a capacity of 4.0 MWh were used in this study to observe the operational performance when subjected to a solar profile [31]. To investigate the operational difference of the case scenarios (Cases 1-4), the power (P) distribution on the first day of the year (January 1, 2018) along with the discharged power from BESS (P_D), H_2^{GEN}, and H_2^{STO} were demonstrated, as shown in Fig. 4, for all the considered cases, respectively. In Case 1, BESS was not connected, as shown in Fig. 1(a). This implies that the total power generated from the solar electricity (P_S) was equal to P, which is the power going to the electrolyzer. Owing to the BESS's absence, there was no production at night, as shown in Fig. 4(a).

However, for Case 2, the split fraction (A) was set as 0.8 and 0.2 for B to ensure the operation of AWE as well as the charging of BESS from solar energy. In contrast, the split fractions (A) for Cases 3, and 4 were set to 0.7 and 0.9, respectively. Based on the proposed operational strategy explained in Fig. 3, Case 2's operation when based on the operational strategy can be seen in Fig. 4(b). Throughout the day, H_2^{GEN} remained greater than zero. The fluctuation caused by the solar power was reduced, but the total hydrogen production was less than the amount generated in Case 1 for a single day due to the operation at lower power from BESS. However, for Case 3, the discharge power from BESS (P_D) was kept variable depending on the BESS's SOC. A higher value of cn was assigned during the hours of more power generation, and less values were assigned during the hours of less power generation. The hydrogen production of Case 3 was almost similar to that of Case 2. Whereas, for Case 4, the hydrogen production was highest, as shown in Fig. 4(d) for one day, as BESS discharged maximum power at night. As BESS discharged maximum power, it soon touched its lower limit and then turned off to avoid complete drainage as a safe operation precaution. When it comes to hydrogen production, the main variables kept under consideration are the split fractions (AWE fraction (A) and BESS fraction (B)) and the discharged power value (cn) from the battery. The upper and lower bounds of the discharge power must be selected considering the battery capacity and operational limits. The same goes for the AWE operational load. The minimum and maximum power values required by AWE must be

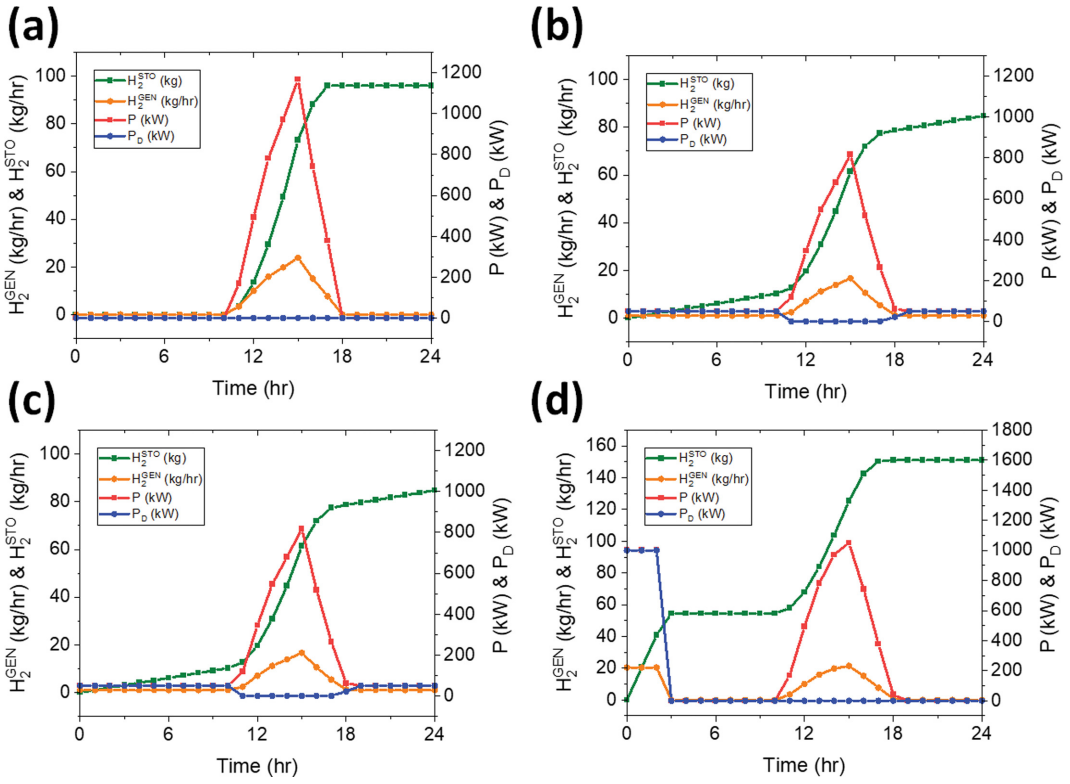

Fig. 4. One day operation for (a) Case 1, (b) Case 2, (c) Case 3, and (d) Case 4.

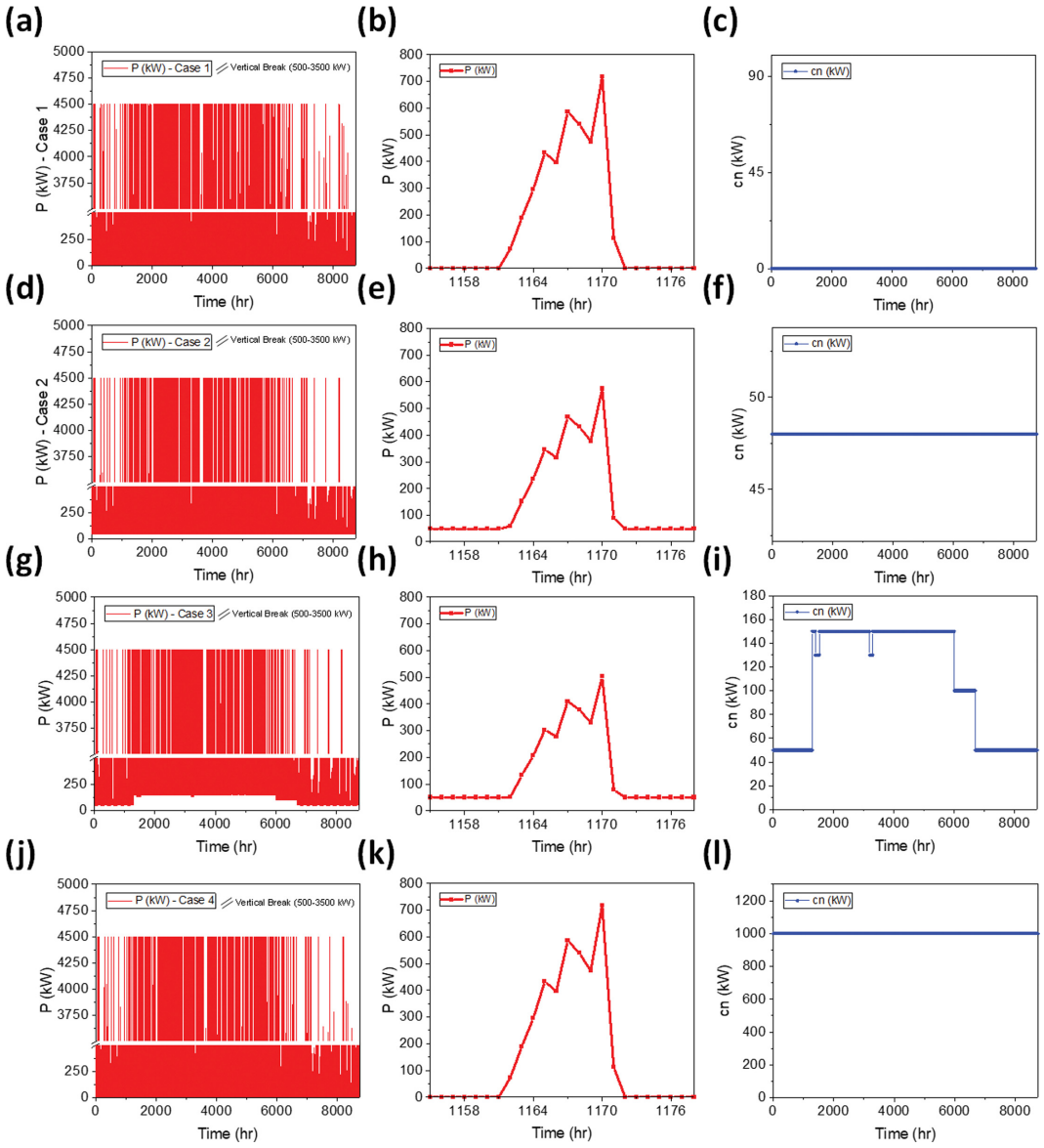

Fig. 5. (a), (d), (g), (j) Power values from the solar PV (P_S) for one whole year at one-hour time interval for Cases 1, 2, 3, and 4, respectively. (b), (e), (h), (k) One-day operational profile from 1,155-1,179 h for Cases 1, 2, 3, and 4, respectively. (c), (f), (i), (l) cn from BESS for Cases 1, 2, 3, and 4, respectively. In Figs. 5(a), (d), (g), and (j), // denotes a vertical break on the y-axis for easier presentation of the results.

kept into consideration. A one-year power (P) distribution to AWE for all the four cases is shown in Fig. 5(a), (d), (g), and (j), respectively, followed by the power (P) to AWE at 1,155-1,179 h, to see a better resolution of a single day in the whole year, as shown in Fig. 5(b), (e), (h), and (k). Lastly, Fig. 5(c), (f), (i), and (l) shows the power discharge from BESS (P_D) for Cases 1, 2, 3, and 4, respectively. cn was zero for Case 1, as there is no BESS. For Case 2, the value of cn was the same throughout the year, and the final power discharged from BESS (P_D) was tabulated as per the operational strategy explained in Section 2.2. For Case 3, the value of cn was manually chosen based on the available SOC. The values were chosen to ensure maximum possible production while keeping continuous operation ($P>P_{MIN}$). However, for Case 4, cn was fixed at the maximum BESS discharge power (1,000 kW).

When comparing the systems over one year, the increase in the annual hydrogen production with and without BESS is quite interesting, as shown in Fig. 6(a), (d), (g), and (j) and Fig. 6(b), (e), (h), and (k) for a better resolution of a single day in the whole year. Case 1 generated the highest hydrogen production without BESS, while Cases 2 and 3 reported the lowest production in comparison with Cases 1 and 4. This is because the solar power was distributed and BESS ensured continuous operation throughout the year (no shutdown). However, Case 4 showed a slightly lower value of H_2^{STO} while operating at maximum power from BESS. Based on the available solar power and AWE capacity, it should be noted that the plant only operated at a capacity factor of 22% for Cases 1 and 4, whereas this value was further decreased to 20% for Cases 2 and 3.

Fig. 6(c), (f), (i), and (l) illustrates the SOC (%) for a period of

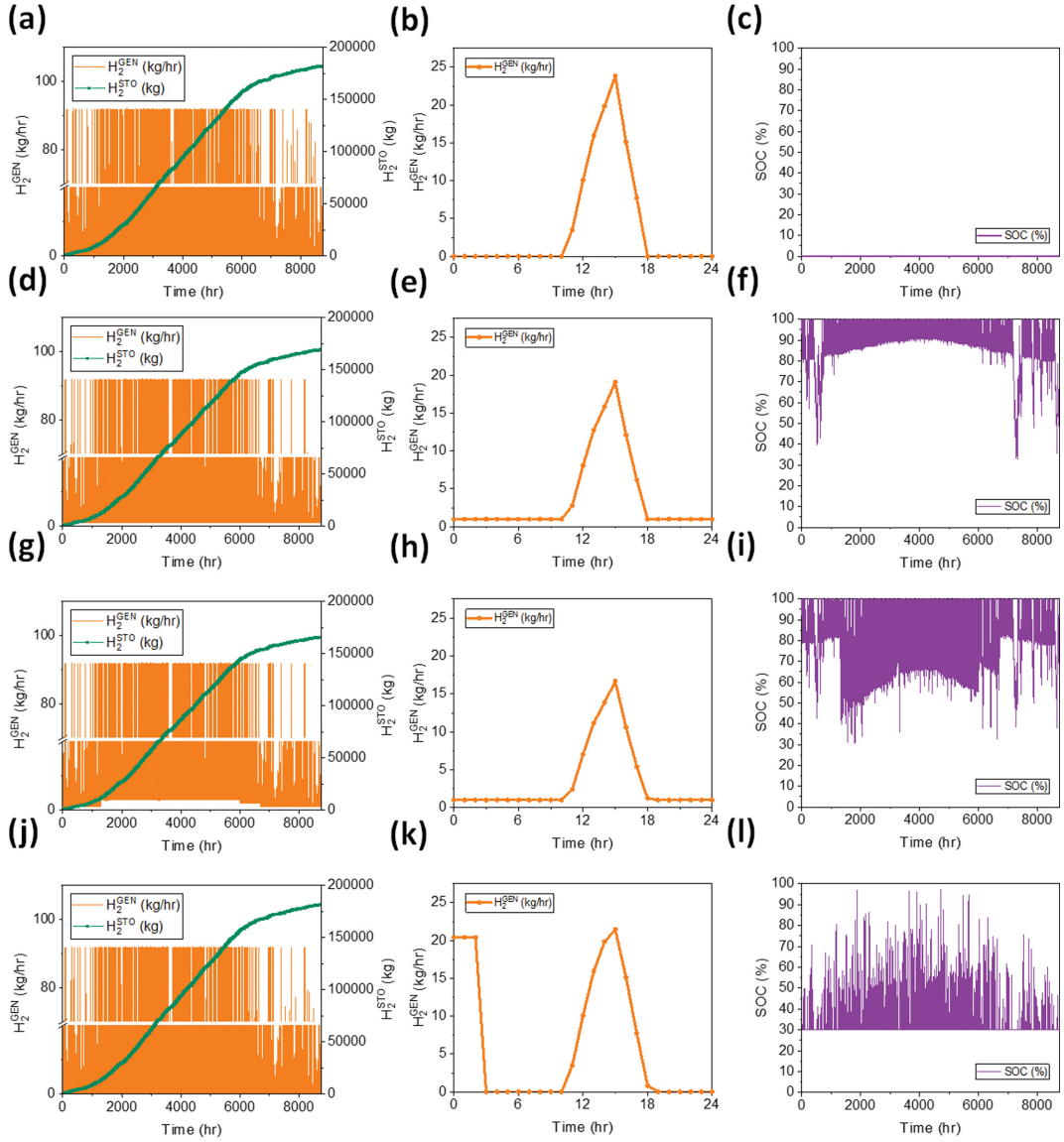

Fig. 6. H_2^{GEN} and H_2^{STO} for a whole year at 1-h time intervals for Cases (a) 1, (d) 2, (g) 3, and (j) 4, respectively. One-day H_2^{GEN} profile from 0-24 h for Cases (b) 1, (e) 2, (h) 3, and (k) 4, respectively. SOC of BESS for Cases (c) 1, (f) 2, (i) 3, and (l) 4, respectively.

one year. As shown in Fig. 6(f), during the initial hours (0-1,500), there was a decline in the SOC (%) curve due to the less solar generation (a winter season), and BESS provided support to AWE to meet the minimum load requirement. After 1,500 hr, an increase could be observed in the SOC (%) curve, representing the start of the summer season, and the battery tended to stay fully charged owing to the ample sunlight for solar power generation. With a bigger BESS capacity, production can be increased by increasing the cn values and adjusting the split fraction (A/B). Moreover, having a BESS could increase the reliability of ensuring continuous production but result in higher LCOH. Whereas, if the operation for AWE and BESS was optimized for maximum production, the results might have been favorable for standalone AWE systems with BESS.

3. Techno-economic Analyses

This analyses evaluated the economic feasibility of using solar PV for hydrogen production using AWE based on the simulated dynamic operation of actual weather data [44]. The size of the solar plant was kept slightly higher than the AWE capacity to overcome solar generation losses. The number of modules required for the solar plant's nameplate capacity was determined using the SAM model. This study considered four different scenarios: Cases 1, 2, 3, and 4.

The costs of the major sections used in the analyses and the total cost were summarized, as shown in Fig. 7. The units consisted of solar PV plant, BESS, AWE, storage, and compression costs. Case 1 did not have BESS; thus, it had less equipment costs compared with Cases 2-4. The total operating cost of the plant was divided into fixed operating costs and variable O&M costs. This cost includes the variable costs related to using deionized water, KOH solution (electrolyte), process steam (used during the run-up to heat the system), and nitrogen (used for cleaning purposes) along with the maintenance and fixed operating costs [44]. A detailed evaluation

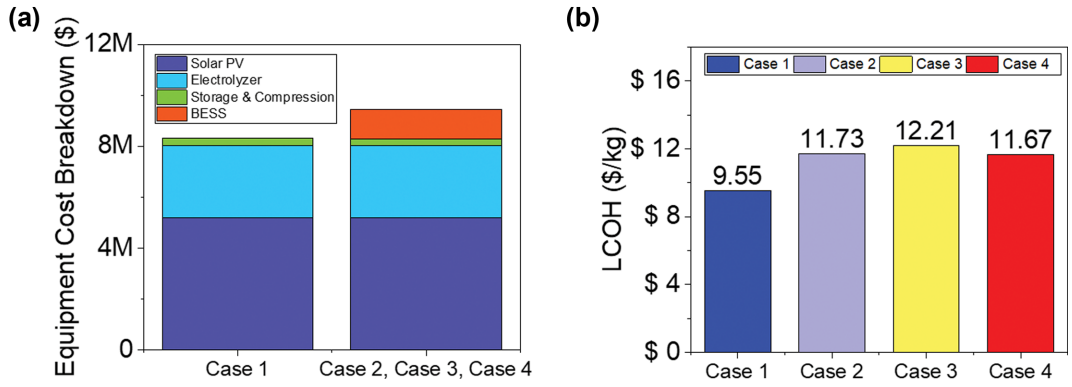

Fig. 7. (a) Equipment cost breakdown for Case 1 vs. Cases 2-4. The electrolyzer includes water treatment, electrics, gas equipment, safety system, and control. The storage and compression costs include electrics, gas equipment, safety system, control, and storage costs. BESS includes the costs for the power ($/kW) and BESS capacity ($/kWh). (b) LCOH for Cases 1-4.

of the year-wise cost was performed in MS Excel. These cost evaluations were then used to calculate LCOH.

Fig. 7(b) shows LCOH for Cases 1-4, respectively. Case 1 had the lowest LCOH of 9.55 $/kg, followed by Case 2 with an LCOH of 11.67 $/kg. Based on the available solar potential in Korea, the plant only operated at a 22% capacity factor in a year with 8760 operational hours. If this capacity factor is increased from the current value to 30% by either optimized operation or through a power purchase agreement, the resulting LCOH would be 7.04 $/kg, which is 27.32% lower than the current reported value. Similarly, for Case 4, a capacity factor of 30% would result in a 25.8% decrease in LCOH.

A discounted payback period for each scenario was evaluated in [45]. The payback period was evaluated at different hydrogen selling prices: (1) at the minimum hydrogen selling price and (2) at a constant price of 21 $/kg for all cases. The results indicated that Case 1 had the fastest payback period of 8 years followed by Case 4 at 11 years. Cases 2 and 3 had the longest payback period. Overall, Case 1 had the fastest payback period among all scenarios, and Case 4 had the fastest payback period among scenarios with BESS. This gives investors a comprehensive overview and allows them to focus on operational reliability, system performance, better econom-

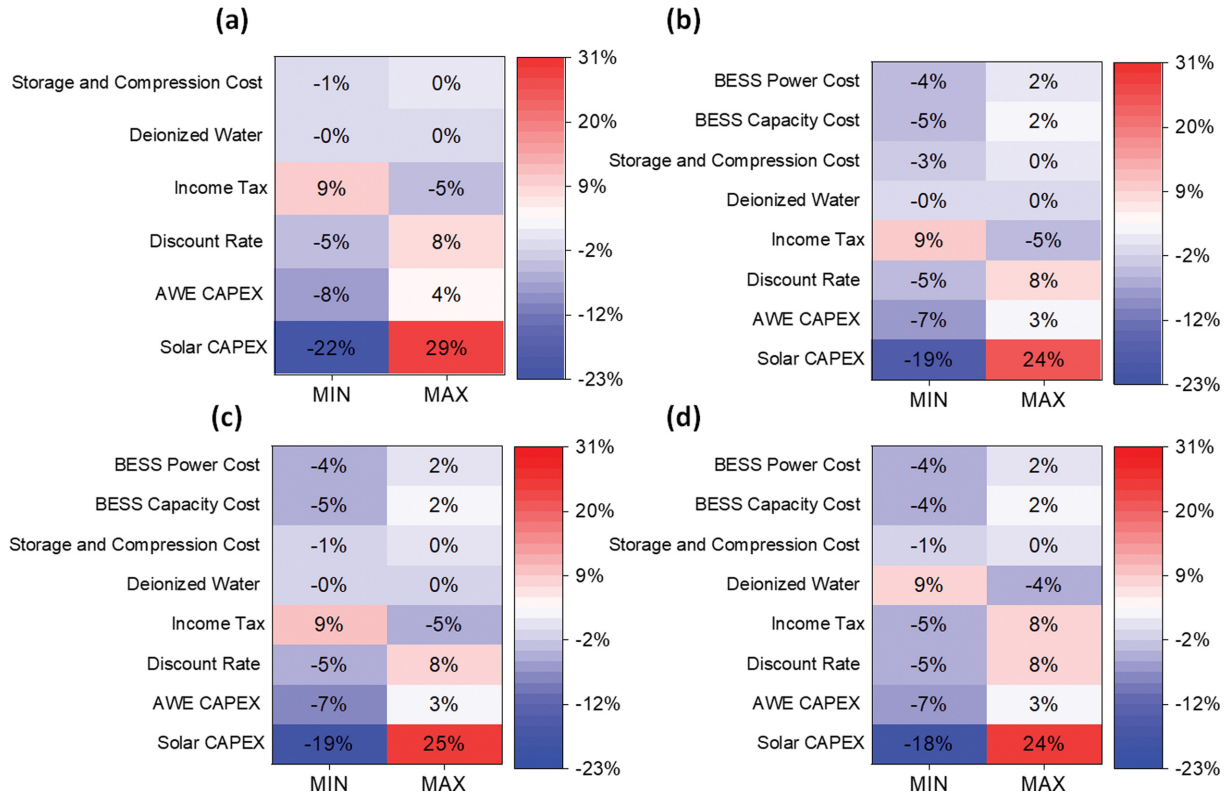

Fig. 8. Sensitivity analysis for the LCOH of Cases (a) 1, (b) 2, (c) 3, and (d) 4.

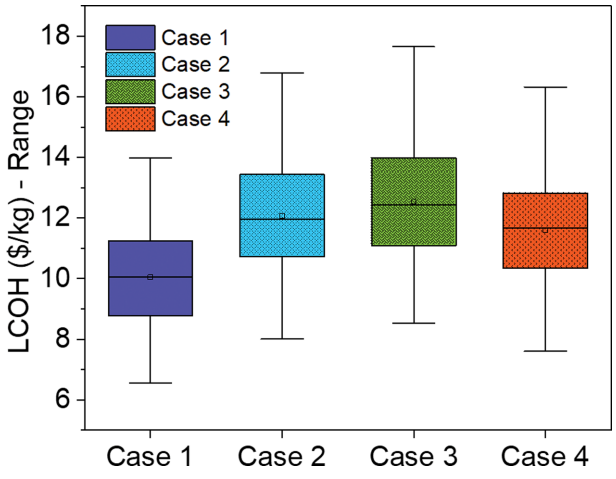

Fig. 9. Monte Carlo simulation results for LCOH of Cases 1-4.

ics, or all factors. Furthermore, optimized operation can lead to a balanced system with greater productivity and increased profit margins.

4. Sensitivity Analyses and Risk Assessment

By varying the parameters between the maximum and minimum possible fluctuations while further studying the effect of the parameters in the techno-economic analyses, a one-point sensitivity analysis was used. The effect of the specific parameters on the hydrogen cost was evaluated, keeping the other parameters fixed. The used parameters in this study were CAPEX for solar, AWE, discount rate, income tax rate, storage and compression costs, and deionized water cost. Heatmaps were demonstrated for all the cases, as shown in Fig. 8. The solar and AWE CAPEX had the highest impact predominantly for all the cases, followed by the discount rate, BESS capacity cost, and BESS power cost. However, the deionized water cost had the lowest impact.

Based on the abovementioned sensitivity parameters, 1,000 possible LCOH and NPV values were determined through the conducted Monte Carlo analysis, and these values are presented for Cases 1-4 along with their reported base LCOH values as box plot shown in Fig. 9. The selected range for the used parameters in the Monte Carlo analyses was the same as described in the sensitivity analysis section. The Monte Carlo analysis for Case 1 showed a minimum value of 6.55 $/kg and a maximum value of 13.99 $/kg for LCOH. However, for Case 4, the minimum possible value for LCOH was 7.60 $/kg, and the maximum value was 16.32 $/kg, which is 13.8% higher than those reported for Case 1. Cases 2 and 3 reported minimum possible LCOH values of 8.01 and 8.53 $/kg. However, their maximum possible LCOH values were 16.79 and 17.65 $/kg.

CONCLUSIONS

Using actual solar data of one year (2018), this study presents an operational strategy and a credible feasibility study based on dynamic operation, offering investor insights into making profitable standalone solar-powered AWEs with energy storage systems. (1) The proposed operational strategy mitigates the operational disturbances resulting from the fluctuating supply of solar energy by providing tangible support from BESS. In addition, it ensures smooth operation and positive production during operational periods. (2) The use of solar data with higher time resolutions provides a more reliable estimate for the solar-based hydrogen production potential in Korea. Furthermore, this study incorporates dynamic operation-based results for economic assessments using actual solar data of Korea. The estimated minimum possible LCOH was reported as 6.55 $/kg for Case 1 and as 7.60 $/kg for Case 4, underlining the potential opportunities available in the renewable energy and hydrogen production sectors from an economic viewpoint. The results highlighted Case 1 as a more cost-effective scenario; however, Cases 2 and 3 make ground for greater operational reliability owing to the presence of BESS. A system without a BESS may be more profitable, but a system with BESS increases operational reliability. To realize a system possessing both economic and operational security, dynamic optimization plays a vital role in optimizing the operational security and maximizing the profit margins. Thus, overall, this study provides a realistic operational and economic perspective of solar AWE and energy storage systems for future hydrogen production investors and policymakers. In addition, this study can be applied to any given location based on actual weather data to estimate the hydrogen generation potential and location-specific economic feasibility. Future work will consider dynamic operation optimization for standalone renewable-powered AWEs with BESS to further explore the cheapest routes of making AWE and BESS profitable.

ACKNOWLEDGEMENTS

This research was supported through a National Research Foundation of Korea (NRF) grant funded by the Ministry of Science and ICT (2019R1A2C2084709). This work was also supported by the Korea Institute of Energy Technology Evaluation and Planning (KETEP) and the Ministry of Trade, Industry, and Energy (MOTIE) of the Republic of Korea (no. 20194010201840).

NOMENCLATURE

PV : photovoltaic
AWE : alkaline water electrolyzer
BESS : battery energy storage system
LCOH : levelized cost of hydrogen
GHG : greenhouse gas emissions
PEM : proton exchange membrane
SAM : system advisor model
SOC : state of charge
V_{rev} : reversible voltage
ΔG : Gibbs energy
z : number of electrons
F : Faraday's constant
V_{cell} : cell voltage
V_{act} : activation voltage
V_{ohm} : Ohmic overvoltage
s : coefficient for overvoltage on electrodes [V]
I : current

t : coefficient for overvoltage on electrodes [$A^{-1}m^2$]
A : area of cell
r : parameter related to ohmic resistance of electrolyte [Ωm^2]
f_1 : parameter related to Faraday efficiency [mA^2cm^{-4}]
f_2 : parameter related to Faraday efficiency
T : Temperature [°C]
η_F : Faradays efficiency
H_2^{GEN} : hydrogen generation
n_c : number of cells
η_{Ele} : efficiency of electrolyzer
P : total power to AWE
P_{MIN} : minimum required power to AWE
P_{MAX} : maximum power to AWE
LHV : lower heating value
H_2O^{cons} : water consumed
O_2^{GEN} : oxygen generated
Q : volumetric flowrate
MW : mega watt
H_2O^{IN} : water going in AWE
H_2O^{OUT} : water going out of AWE
O_2^{IN} : oxygen going in AWE
O_2^{OUT} : oxygen going out of AWE
H_2^{IN} : hydrogen going in AWE
H_2^{OUT} : hydrogen going out of AWE
H_2O^{CONS} : water consumed
H_2O^{GEN} : water generated
H_2^{STO} : hydrogen stored
P_C : charging power of BESS
P_D : discharging power of BESS
$P_{C_{MIN}}$: minimum charging power of BESS
$P_{C_{MAX}}$: maximum charging power of BESS
$P_{D_{MIN}}$: minimum discharging power of BESS
$P_{D_{MAX}}$: maximum discharging power of BESS
SOC_{MIN} : minimum state of charge
SOC_{MAX} : maximum state of charge
η^+ : charging efficiency
η^- : discharging efficiency
t : time
P_S : solar power
A/B : spit fractions, A for AWE, B for BESS
P_A : power split to AWE
P_C : power split to BESS
P_X : excess power generated
CI : cost index
IRR : internal rate of return
FCI : fixed capital investment
TIC : total installed cost
TLCC : total life cycle cost
NPV_{OP} : net present value of other products
D : discount rate
n : analysis year
L : analysis period - 30 years

SUPPORTING INFORMATION

Additional information as noted in the text. This information is available via the Internet at http://www.springer.com/chemistry/journal/11814.

REFERENCES

1. P. A. Owusu and S. Asumadu-Sarkodie, *Cogent Eng.*, **3**, 1167990 (2016).
2. J. S. T. Pedersen, F. D. Santos, D. van Vuuren, J. Gupta, R. E. Coelho, B. A. Aparício and R. Swart, *Glob. Environ. Chang.*, **66**, 102199 (2021).
3. P. D. Zakkour, W. Heidug, A. Howard, R. S. Haszeldine, M. R. Allen, D. Hone and R. S. Haszeldine, *Taylor Fr.*, **21**, 63 (2020).
4. O. Nematollahi and K. C. Kim, *Renew. Sustain. Energy Rev.*, **77**, 566 (2017).
5. W. Won, H. Kwon, J. H. Han and J. Kim, *Renew. Energy*, **103**, 226 (2017).
6. S. Cho and J. Kim, *Korean J. Chem. Eng.*, **33**, 2808 (2016).
7. I. Renewable Energy Agency, Green hydrogen: A guide to policy making (2020).
8. M. A. Qyyum, R. Dickson, S. F. Ali Shah, H. Niaz, A. Khan, J. J. Liu and M. Lee, *Renew. Sustain. Energy Rev.*, **145**, 110843 (2021).
9. Y. H. Jia, J. Y. Choi, J. H. Ryu, C. H. Kim, W. K. Lee, H. T. Tran, R. H. Zhang, D. H. Ahn, T. X. Bac and T. Xuan, *Korean J. Chem. Eng.*, **27**, 1854 (2010).
10. M. Lee and J. Kim, *Korean J. Chem. Eng.*, **34**, 1604 (2017).
11. C. Schnuelle, T. Wassermann, D. Fuhrlaender and E. Zondervan, *Int. J. Hydrogen Energy*, **45**, 29938 (2020).
12. F. Dawood, G. M. Shafiullah and M. Anda, *Sustainability*, **12**, 2047 (2020).
13. R. Andika, Y. Kim, C. M. Yun, S. H. Yoon and M. Lee, *Korean J. Chem. Eng.*, **36**, 12 (2019).
14. H. Niaz, B. Brigljevic, Y. B. Park, H. C. Woo and J. J. Liu, *ACS Sustainable Chem. Eng.*, **8**(22), 8305 (2020).
15. D. Gielen, E. Taibi and R. Miranda, *Hydrogen: A renewable energy perspective*, International Renewable Energy Agency (IRENA) (2019).
16. Ø. Ulleberg, *Int. J. Hydrogen Energy*, **28**, 21 (2003).
17. F. I. Gallardo, A. M. Ferrario, M. Lamagna, E. Bocci, D. A. Garcia and T. E. Baeza-Jeria, *Int. J. Hydrogen Energy*, **46**, 13709 (2020).
18. F. Gutiérrez-Martín, L. Amodio and M. Pagano, *Int. J. Hydrogen Energy*, In press (2020), https://doi.org/10.1016/j.ijhydene.2020.09.098.
19. A. Mostafaeipour, H. Rezayat and M. Rezaei, *Int. J. Hydrogen Energy*, **45**, 31599 (2020).
20. A. Kovač, D. Marciuš and L. Budin, *Int. J. Hydrogen Energy*, **44**, 9841 (2019).
21. C. A. Rodriguez, M. A. Modestino, D. Psaltis and C. Moser, *Energy Environ. Sci.*, **7**, 3828 (2014).
22. R. Bhattacharyya, A. Misra and K. C. Sandeep, *Energy Convers. Manag.*, **133**, 1 (2017).
23. M. H. Shams, M. Shahabi, M. MansourLakouraj, M. Shafie-khah and J. P. S. Catalão, *Energy*, **222**, 119894 (2021).
24. A. Grimm, W. A. de Jong and G. J. Kramer, *Int. J. Hydrogen Energy*, **45**, 22545 (2020).
25. B. Lee, J. Heo, S. Kim, C. Sung, C. Moon, S. Moon and H. Lim, *Energy Convers. Manag.*, **162**, 139 (2018).
26. B. Lee, H. Lee, H. S. Cho, W. C. Cho, C. H. Kim and H. Lim, *Sus-*

tain. Energy Fuels, **3**, 1799 (2019).
27. M. H. Shams, M. Kia, A. Heidari and D. Zhang, *Simulation*, **95**, 931 (2019).
28. N. Blair, A. P. Dobos, J. Freeman, T. Neises, M. Wagner, T. Ferguson, P. Gilman and S. Janzou, *NREL Rep. No. TP-6A20-61019, Natl. Renew. Energy Lab. Golden, CO*, 13 (2014).
29. A. Rabiee, A. Keane and A. Soroudi, *Renew. Energy*, **163**, 1580 (2021).
30. M. Cerchio, F. Gullí, M. Repetto and A. Sanfilippo, *Electronics*, **9**, 1734 (2020).
31. A. Mayyas and M. Mann, *DOE Hydrog. Fuel Cells Progr.*, June (2018).
32. R. Turton, R. C. Bailie, W. B. Whiting and J. A. Shaeiwitz, *Analysis, synthesis and design of chemical processes*, Pearson Education (2008).
33. J. I. Levene, M. K. Mann, R. M. Margolis and A. Milbrandt, *Sol. Energy*, **81**, 773 (2007).
34. L. Bertuccioli, A. Chan, D. Hart, F. Lehner, B. Madden and E. Standen, Development of Water Electrolysis in the European Union (2014).
35. G. Parks, R. Boyd, J. Cornish, R. Remick and I. Review Panel, Hydrogen Station Compression, Storage, and Dispensing Technical Status and Costs: Systems Integration (2020).
36. B. Brigljević, P. Fasahati and J. Jay Liu, *Comput. Aided Chem. Eng.*, **44**, 337 (2018).
37. L. Vimmerstedt, S. Akar, C. Augustine, P. Beiter, W. Cole, D. Feldman, P. Kurup, E. Lantz, R. Margolis, A. Ramdas, T. Stehly, C. Turchi and D. Oladosu, 2019 Annual Technology Baseline, Golden, CO (United States) (2019).
38. J. Y. Lim, U. Safder, B. S. How, P. Ifaei and C. K. Yoo, *Appl. Energy*, **283**, 116302 (2021).
39. R. Dickson, J.-H. Ryu and J. J. Liu, *Energy*, **164**, 1257 (2018).
40. S. H. Lee, D.-H. Lim and K. Park, *Appl. Sci.*, **10**, 5391 (2020).
41. W. Short, D. Packey and T. Holt, *Renew. Energy*, **95**, 73 (1995).
42. L. Vimmerstedt, S. Akar, C. Augustine, P. Beiter, W. Cole, D. Feldman, P. Kurup, E. Lantz, R. Margolis, A. Ramdas, T. Stehly, C. Turchi and D. Oladosu, 2019 Annual Technology Baseline, Golden, CO (2019).
43. H. Kojima, T. Matsuda, H. Matsumoto and T. Tsujimura, *J. Int. Counc. Electr. Eng.*, **8**, 19 (2018).
44. A. Nicita, G. Maggio, A. P. F. Andaloro and G. Squadrito, *Int. J. Hydrogen Energy*, **45**, 11395 (2020).
45. M. Rezaei, N. Naghdi-Khozani and N. Jafari, *Renew. Energy*, **147**, 1044 (2020).
46. B. Lee, J. Heo, N. H. Choi, C. Moon, S. Moon and H. Lim, *Int. J. Hydrogen Energy*, **42**, 24612 (2017).
47. M. Felgenhauer and T. Hamacher, *Int. J. Hydrogen Energy*, **40**, 2084 (2015).
48. S. Nistor, S. Dave, Z. Fan and M. Sooriyabandara, *Appl. Energy*, **167**, 211 (2016).
49. J. Hinkley, J. Hayward, R. Mcnaughton, R. Gillespie, M. Watt and K. Lovegrove, Cost assessment of hydrogen production from PV and electrolysis (2016).

Supporting Information

Techno-economic feasibility evaluation of a standalone solar-powered alkaline water electrolyzer considering the influence of battery energy storage system: A Korean case study

Haider Niaz, Mohammad MansourLakouraj, and Jay Liu†

Department of Chemical Engineering, Pukyong National University, Busan 48513, Korea
(*Received 23 January 2021 • Revised 20 April 2021 • Accepted 23 April 2021*)

Table S1. Technical details for the weather data, solar module, inverter and system design for the AWE model from SAM

Weather data information	
Data source	NSRDB
Station ID	785765
Latitude	50.37
Longitude	−92.9
Time zone	GMT-6
Elevation	367 m
Annual average values from weather file	
Direct normal (kWh/m^2/day)	3.79
Diffuse horizontal (kWh/m^2/day)	1.30
Average temperature (C)	1.4
Average wind speed (m/s)	0.7
Solar module	
Name	SunPower SPR-X21-350-BLK-E-AC
Technology	Mono-c-Si
Nominal efficiency (%)	21.4787
Maximum power (Wdc)	350.103
Max power voltage (Vdc)	57.3
Max power current (Adc)	6.1
Open circuit voltage (Vdc)	68.2
Open circuit current (Adc)	6.5
Module area (m^2)	1.630
Number of cells	96
Number of solar panels (units)	18564
Land required for solar panels (acres)	24.9
Inverter	
Name	SMA America: STP-60-US-10 [400V]
Maximum AC power (Wac)	59860
Maximum DC power (Wdc)	61130.8
Nominal AC voltage (Vac)	400
Nominal DC voltage (Vdc)	800
Maximum DC current (Adc)	97.033

Table S2. Simulation parameters and constants

Constant parameters	Symbols	Units	Value
Reversible voltage	V_{rev}	V	1.229
Area of electrode (Total Plate Solid Area)	A	cm^2	400
Single cell amps		A	520
Current density		A/cm^2	0.20
Cells per system			573
Stacks per system			3
Cells per stack			191
Faraday's constant	F	C/mol	96485
Number of electrons	z		2
Coefficient for overvoltage on electrodes	s	V	0.185
	t_1	$A^{-1}m^2$	1.002
Coefficient for overvoltage on electrodes	t_2	$A^{-1}m^{2o}C$	8.424
	t_3	$A^{-1}m^{2o}C$	247.3
Parameter for ohmic resistance of electrolyte	r_1	Ωm^2	8.05e-5
	r_2	$\Omega m^{2o}C^{-1}$	-2.5e-7

Table S3. Assumptions for the calculation of fixed capital investment and operating cost

Total Installation Cost (TIC)	Variable	%
Buildings (1% of TIC)	a	1.0%
Site Development (9% of TIC)	b	9.0%
Additional Piping (4.5% of TIC)	c	4.5%
Total Direct Cost (TDC)	TDC	a+b+c

Indirect Costs	Variable	%
Prorated Expenses (10% of TDC)	d	10.0%
Home Office and Construction Fees (20% of TDC)	e	20.0%
Field Expenses (10% of TDC)	f	10.0%
Project Contingency (10% of TDC)	g	10.0%
Startup and Permits (5% of TDC)	h	5.0%
Total Indirect Costs (TIC)	TIC	d+e+f+g+h

Fixed Capital Investment	FCI	TDC+TIC
Land	i	5% of TIC
Working Capital	j	5% of FCI

Fixed Operating Cost	Variable	Total Cost (US M$)/Year
Plant Manager	FOC	0.15
Plant Engineer		0.07
Maintenance Supervisor		0.06
Lab Manager		0.06
Shift Supervisor		0.24
Lab Technician		0.16
Maintenance Tech		0.28
Shift Operators		1.20
Yard Employees		0.11
Clerks		0.04
Total (US-$)		$ 2.37
Variable Operating Cost	n	
Overhead and Maintenance (1.6% of TIC)	k	1.6% * TIC
Maintenance Capital (3% of TIC)	l	0.03% * TIC
Insurance and Taxes (0.7% of FCI)	m	0.7% * TIC
Total Other Fixed Costs	OFC	FOC+k+l+m
Total Operating Cost		n+OFC